Nanoscale Res Lett (2009) 4:1178–1182
DOI 10.1007/s11671-009-9382-y

NANO EXPRESS

# Characterization of Titania Incorporated with Alumina Nanocrystals and Their Impacts on Electrical Hysteresis and Photoluminescence

**Lei Shi · Zhiguo Liu · Bo Xu · Ligang Gao · Yidong Xia · Jiang Yin**

Received: 14 March 2009 / Accepted: 15 June 2009 / Published online: 28 June 2009


**Abstract** The structural and optical characterizations of titania incorporated with alumina nanocrystals have been presented in this paper and the films exhibit excellent properties like low current density, small hysteresis as well as high photoluminescence quantum yields of about 361 nm. These properties are promising for the applications in future electronic devices.

**Keywords** Nanocrystal · Electrical hysteresis · Photoluminescence · Pulsed laser deposition

## Introduction

During the past few years, many metal-oxide nanocrystals have attracted much attention because of their interesting electronic and optical properties for a wide range of applications. For example, $SnO_2$ nanocrystals by doping with various additives have shown perfect detection of analytes in *ppm* concentration and long-term stability as metal-oxide gas sensors [1–3]. Similarly, $ZnO_2$ nanocrystals have demonstrated the efficient blue-green emission for fluorescence-based applications [4, 5]. The research on new oxide materials with homogeneous nanocrystals is of key importance in order to achieve optimum performance in different electronic devices.

L. Shi · Z. Liu (✉) · B. Xu · L. Gao · Y. Xia · J. Yin
National Laboratory of Solid State Microstructures, Nanjing University, Hankou Road 22, 210093 Nanjing, People's Republic of China
e-mail: liuzg@nju.edu.cn

L. Shi
e-mail: shl7900@yahoo.com.cn

The amazing potential for these nano-size materials arise from the fact that it is possible to fabricate structures of radius smaller than the electron hole pair (exciton) Bohr radius [6, 7]. Because of the quantum confinement effect, the charge carriers can strongly be confined in nanocrystals. Therefore, the band gap will increase obviously as compared with the bulk material. Furthermore, in the confinement region, the band gap is conveniently tuned by virtue of adjusting the nanocrystal diameter to achieve some special electrical or optical properties. This particular property of nanocrystals supplies with the prime motivation to further investigate and optimize the new oxide materials.

Recently, it has been found that titania-incorporated alumina pseudobinary films as the next generation gate dielectrics can enlarge the band gap and restrain the exceeding leakage current [8]. Although these properties are very attractive for the alternative gate dielectrics, it has also been reported that during high temperature (approach to the crystallization temperature) annealing of the amorphous films, the composition may decompose into some nanocrystals, and this may degrade the electrical characteristics of the gate dielectric, especially, for the pseudobinary system [9, 10]. Unfortunately, the thermal treatment is inevitable for current complementary metal-oxide semiconductor (CMOS) technique. In this regard, the electrical and optical properties of the $Ti_xAl_{1-x}O_y$ films with thermal treatment might differ largely from the amorphous films in the case of the existence of the nanocrystals.

## Materials and Methods

Through a large number of experiments of the pseudobinary titania/alumina system, the deposition conditions and

the film composition have been optimized. Here, we describe the characterization of the $Ti_{0.25}Al_{0.75}O_x$ thin films grown on *n* type silicon (100) substrates by a pulsed laser deposition procedure. The dense $Ti_{0.25}Al_{0.75}O_x$ target used in the experiment was prepared by a solid-state reaction process with pure starting materials of $Al_2O_3$ and $TiO_2$ in a mole ratio of 1.5:1. The mixed powder in this ratio was ball-milled for 24 h, and then sintered at 1,500 °C for 7 h to form a dense ceramic target. The $Ti_{0.25}Al_{0.75}O_x$ thin films were deposited on silicon substrates with $\rho = 2$–3 Ω cm at 400 °C in a chamber of a low oxygen partial pressure $6.0 \times 10^{-5}$ Pa. A KrF excimer laser (COMPex, Lambda Physik, 248 nm in wavelength, 30 ns in pulse width) running at 5 Hz with an average energy density of about 1.6–2.0 J/cm$^2$ per pulse was employed. The distance between the substrate and the target was about 8 cm. The silicon substrates were ultrasonically cleaned by acetone and de-ionized water. Afterward the silicon substrates were immersed in the diluted hydrofluoric acid solution to remove the native silicon dioxide, thus leaving a hydrogen-terminated silicon surface. After the deposition, the amorphous films were in situ annealed at 400 °C in the chamber for 20 min to reduce the defects in the films. Based on the earlier research, the crystallization temperature of the film is a bit higher than 800 °C [11]. Therefore, the deposited films were then annealed at 800 and 900 °C in the hermetic quartzose tubes full of argon for 1 h, respectively (named as S-1 and S-2 below). The samples were characterized by high-resolution transmission electron microscopy (HRTEM), current–voltage (*I–V*) measurement, and photoluminescence (PL) excitation spectroscopy. The PL excitation measurement was carried out using excitation source of 255 nm of xenon lamp at room temperature. Samples with different thicknesses according to the different measurements were prepared in the same procedure.

## Results and Discussion

The 50-nm-thick pseudobinary $Ti_{0.25}Al_{0.75}O_x$ films were post-annealed at 800 and 900 °C after deposition, respectively. The cross-sectional HRTEM image of the S-1 is shown in Fig. 1. A representative image displays a fairly smooth interface layer between the film and the silicon substrate. Some changes have appeared in the bulk of the S-1 after post-annealing treatment. There are several observable bright/dark contrast fluctuations in the film. The electron diffraction pattern of the S-1 as inset of Fig. 1 has shown a typical amorphous halo, which indicates the film is still in amorphous state. Therefore, it could be deduced that these locations are some composition-rich regions, even a few small nanocrystals. When the films have been annealed approaching to the crystallization temperature, the grain coarsening has occurred, and the increase in grain size has been observed.

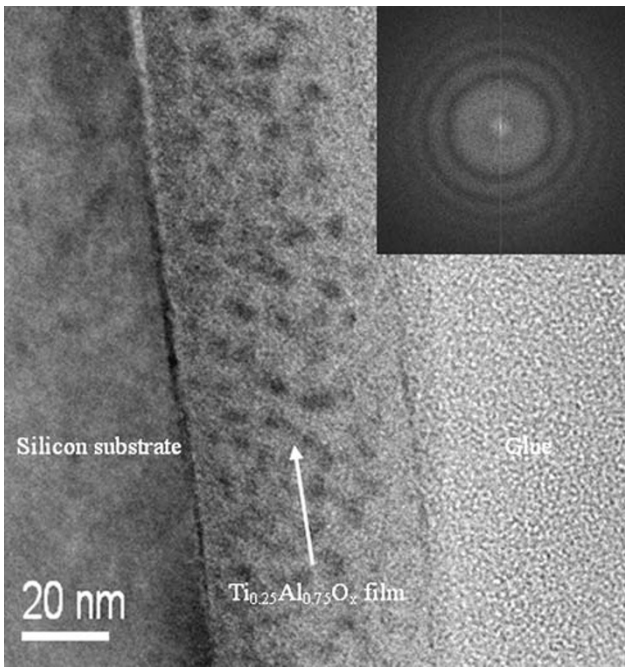


**Fig. 1** HRTEM cross-section image of S-1. *Inset* electron diffraction image of S-1

In comparison, several crystal regions have been observed in the HRTEM image of the S-2 and are shown in Fig. 2. The fast Fourier transformation (FFT) measurement has been carried out on these regions to obtain the complex situations of these nanocrystals, and the relevant image is shown in the right as inset figure. From the figure one can observe that it is a mixed nanocrystal region, because the diffraction pattern is a superposition of the patterns from two pieces of nanocrystals. Both of interplanes spacings, whose values are about 0.237 nm and lie at an angle of near to 60°, are of regular parallelogram with a center and corresponding to the $(\bar{1}01)$ and $(1\bar{1}0)$ planes of the hexagonal $Al_2O_3$, respectively. As for the other dots, the evaluated two interplanes spacings are equivalent to 0.242 nm. It is presumed that the two spots correspond to the (004) and $(00\bar{4})$ planes of orthorhombic $TiAl_2O_5$, respectively.

As indicated above, the HRTEM cross-section and electron diffraction patterns of the $Ti_{0.25}Al_{0.75}O_x$ films demonstrated the formation of nano-sized crystals. Only one-dimensional diffraction patterns of orthorhombic $TiAl_2O_5$ phase in the images indicate that the nanocrystals of the film preferably promote epitaxial *c*-axis-oriented growth. This promotion has been demonstrated by the results derived from the X-ray diffraction [11]. With the X-ray diffraction results, only a small crystal peak attributed to the orthorhombic $TiAl_2O_5$ phase could be observed.

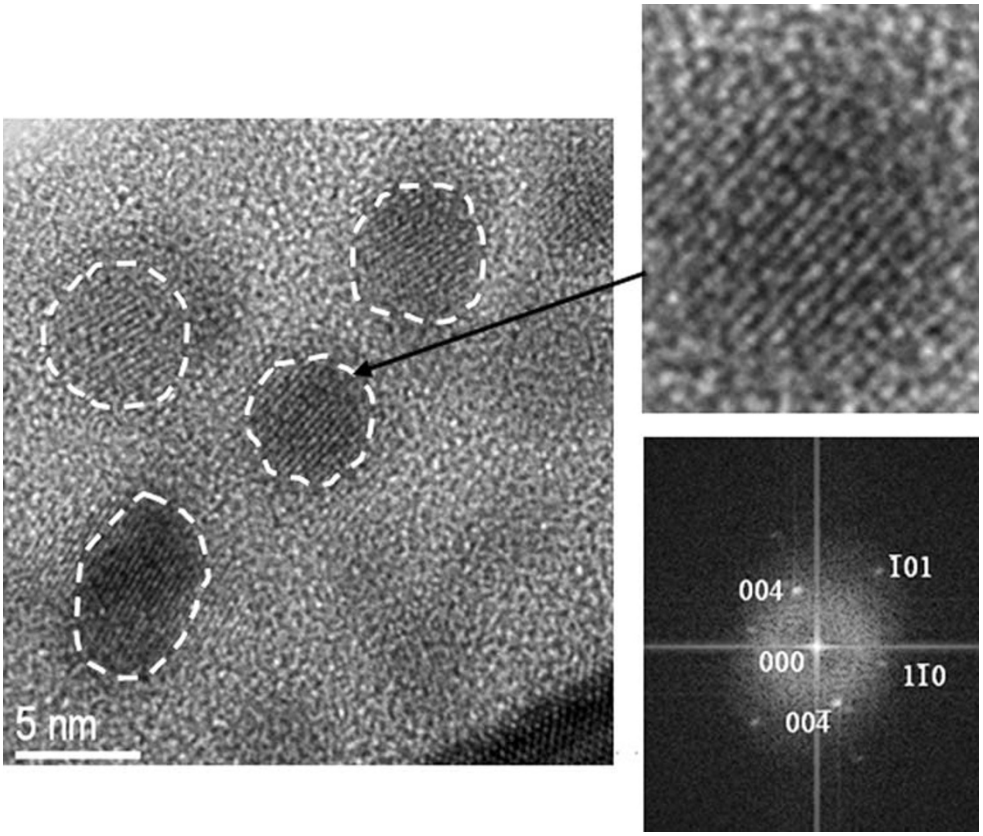


**Fig. 2** HRTEM cross-section image of S-2. The *inset* on the *right* shows the magnified image and the FFT image of the selected nanocrystals

From the macroscopical aspect, the preferable orientation is obvious, and the crystallization of the $Ti_{0.25}Al_{0.75}O_x$ film is anisotropic. Because of the nonstoichiometric composition, no evidence of the presence of $TiO_2$ nanocrystals was detected in this sample.

The typical *I–V* measurements performed on the respective samples are shown in Fig. 3a, b. The S-1 has very good insulating properties, as apparent from the substantial current of about $10^{-6}$ A/cm$^2$ at an electric field of −2 MV/cm applied between the silicon substrate and the metal contact. Comparably, the S-2 exhibits a significantly increased leakage current of $10^{-2}$ A/cm$^2$ at the same electric field, which is almost as much as 4 orders of magnitude derived from S-1. The large leakage currents of S-2 possibly originate from the formation of nanocrystals. Considering the HRTEM results, this confirms the crucial role of the amorphous $Al_2O_3$ in the insulating properties of the dielectric stack, despite its small amount and thickness.

However, the sweep loop characteristics of the investigated samples disclose the hysteresis. It is ascribed to traps located within the bulk $Ti_{0.25}Al_{0.75}O_x$ film or near the $Ti_{0.25}Al_{0.75}O_x$ film/silicon interface, such as oxygen vacancies and the other defects, which get filled with electrons from the applied electrical field upon sweeping to

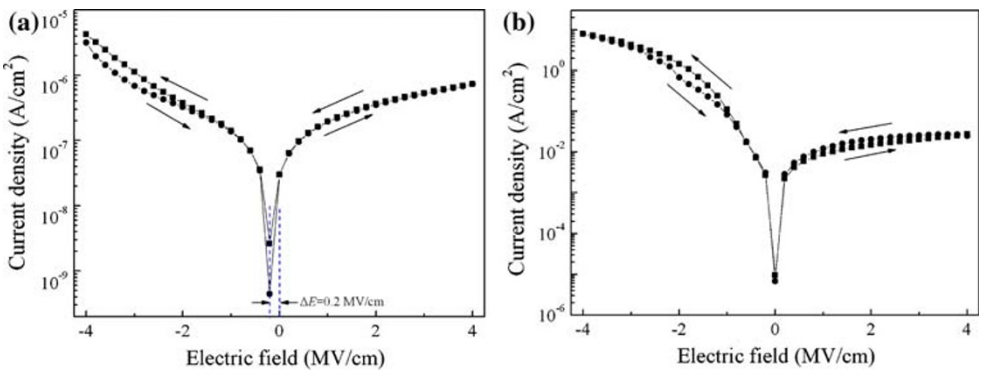


**Fig. 3** Current density versus bias electric field for **a** S-1 and **b** S-2 at room temperature

more positive gate voltages. At room temperature, the hysteresis of S-1 is larger than that of S-2. Such a decrease in hysteresis with annealing temperature reveals the presence of trap charging upon the temperature factor. Moreover, in the absence of applied electrical field, the negative shift ($\sim$0.2 MV/cm) of S-1 proves the existence of positive charges in the bulk film as well. By virtue of its capacitance–voltage curves (not shown here), it is calculated that the oxide trapped charges density is about as much as $10^{12}/cm^2$.

As we all known, Raman spectrum provides a fast and convenient method to detect the small structural changes. Typical Raman spectra from S-1 and S-2 are shown in Fig. 4 that show the same peaks at about 618 $cm^{-1}$ and 814 $cm^{-1}$, which are usually detected in amorphous Ti–O materials, and ascribed to Ti–O stretching and Ti–O–Ti stretching, respectively [12, 13]. The latter stretching may also have contributions from a Ti–O stretch assigned to a short Ti–O bond. Therefore, the large intensity of this peak indicates the a two dimensional connectivity and provides the evidence of the presence of –Ti–O–Ti– chainlike structure with a shortening Ti–O bond distance. The other peak for S-2 at $\sim$1,080 $cm^{-1}$ is the signature of $TiAl_2O_5$ phase [14]. Its full width at half maximum (FWHM) of 50 $cm^{-1}$ is in contrast to the S-1 of FWHM = 40 $cm^{-1}$ at the similar peak region. The Raman linewidth broadening, primarily caused by phonons confinement in nanocrystals, is inversely proportional to the size of the nanocrystals.

In order to further understand the nature of the charge carrier trapping, migration and transfer in $Ti_{0.25}Al_{0.75}O_x$ films with small nanocrystals and the PL excitation spectroscopy with the emission wavelength fixed at 255 nm were performed for the sample S-2. In general, it is difficult to observe the photoluminescence phenomenon at room

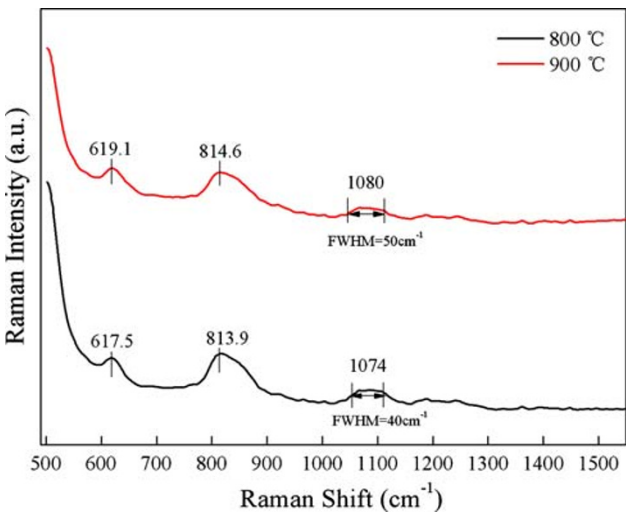


**Fig. 4** Optical Raman spectra for S-1 and S-2

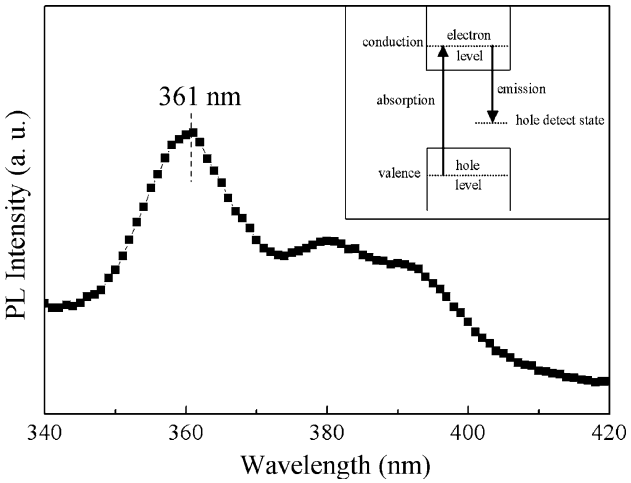


**Fig. 5** Photoluminescence emission spectra for S-2, excitation wavelength 255 nm. *Inset* the energy band structure of the sample

temperature for bulk $TiO_2$ due to its indirect transition nature. However, some nano-sized $TiO_2$ particles and mesoporous-structured powders have been reported to exhibit room temperature photoluminescence [15]. Figure 5 shows the PL excitation spectroscopy of a broad excitation peak centered at $\sim$361 nm. The samples exhibit the very small Stokes shift between the absorption and the emission, which characterizes the energy relaxation resulting from interfacial roughness, defects, and other structural imperfection. Herein, the main probability lies in the defects of nanoclusters and/or nanocrystals in the bulk film. Generally, the electrons are trapped by oxygen vacancies or confined within quantum dots in nanocrystals region. On the other hand, the excited electrons can transfer from the valance band to the new levels that exist upper of the conduction band introduced by the dopant. Thus, the photoluminescence efficiency will be restrained with the thermal treatment. Nevertheless, such a meaningful value has not been previously reported for nanostructural films comprising titania and alumina, and its realization within the present films is notable consideration that no attempts were made to control the size of the nanocrystals.

## Conclusions

In conclusion, we have performed a systematical analysis of titania-incorporated alumina nanocrystals. The present experiments demonstrate that the nanocrystals exhibit excellent properties like low current density and small hysteresis. Moreover, they offer high photoluminescence quantum yields at room temperature. This approach can be extended to other conditions such as low temperature, anion doping, and crystal size controlling.

**Acknowledgments** This work was sponsored by National Natural Science Foundation of China (Grant number of 60576023 and 60636010), the State Key Program for Basic Research of China (2004CB619004), the State Key Program for Science and Technology of China (2009ZX02101-4) and Jiangsu Province Planned Projects for Postdoctoral Research Funds (0204003426).

## References

1. G.S. Pang, S.G. Chen, Y. Koltypin, A. Zaban, S.H. Feng, A. Gedanken, Nano. Lett. **1**(12), 723 (2001)
2. D.F. Zhang, L.D. Sun, J.L. Yin, C.H. Yan, Adv. Mater. **15**, 1022 (2003)
3. A. Tricoli, M. Graf, S.E. Pratsinis, Adv. Funct. Mater. **18**, 1 (2008)
4. S. Rakshit, S. Vasudevan, ACS. Nano. **2**(7), 1473 (2008)
5. D.M. Bagnall, Y.F. Chen, Z. Zhu, T. Yao, M.Y. Shen, T. Goto, Appl. Phys. Lett. **73**, 1038 (1998)
6. D.L. Klein, R. Roth, A.K.L. Lim, A.P. Alivisatos, P.L. McEuen, Nature **389**, 699 (1997)
7. A. Sashchiuk, L. Amirav, M. Bashouti, M. Krueger, U. Sivan, E. Lifshitz, Nano. Lett. **1**(4), 159 (2004)
8. L. Shi, J. Yin, K.B. Yin, F. Gao, Y.D. Xia, Z.G. Liu, Appl. Phys. A: Mater. Sci. Process. **90**(2), 379 (2008)
9. H. Kim, P.C. Mclntyre, J. Appl. Phys. **92**, 5094 (2002)
10. G. Lucovsky, G.B. Rayner Jr, Appl. Phys. Lett. **77**, 2912 (2000)
11. L. Shi, Y.D. Xia, B. Xu, Z.G. Liu, J. Appl. Phys. **101**, 034102 (2007)
12. M. Fernadndez, X.Q. Wang, C. Belver, J.C. Hanson, J.A. Rodriguez, J. Phys. Chem. C. **111**, 674 (2007)
13. L.S. Hsu, R. Rujkorakarn, J.R. Sites, Y. She, J. Appl. Phys. **59**, 3475 (1986)
14. G. Mestl, N.F.D. Verbruggen, F.C. Lange, B. Tesche, H. Knoezinger, Langmuir **12**, 1817 (1996)
15. D. Li, H. Haneda, S. Hishita, N. Ohashi, Chem. Mater. **17**, 2596 (2005)